

# Microscopic Effective Theory for Iron-Based Superconductors

Jiangping Hu<sup>1,2</sup> and Ningning Hao<sup>1,2</sup>

<sup>1</sup>*Beijing National Laboratory for Condensed Matter Physics,  
Institute of Physics, Chinese Academy of Sciences, Beijing 100080, China*

<sup>2</sup>*Department of Physics, Purdue University,  
West Lafayette, Indiana 47907, USA*

## Abstract

Although iron-based superconductors are multi-orbital systems with complicated band structures, we demonstrate that the low energy physics which is responsible for high- $T_c$  superconductivity is essentially governed by two almost decoupled single-orbital effective Hamiltonians near half filling. This underlining electronic structure is protected by the  $S_4$  point group symmetry at iron sites. The model results in a robust  $A_{1g}$  s-wave pairing which can be exactly mapped to the d-wave pairing observed in cuprates, the high  $T_c$  Cu-oxide superconductors. Our derivation provides an unified understanding of iron-pnictides and iron-chalcogenides, and suggests that cuprates and iron-based superconductors share identical high- $T_c$  superconducting mechanism.

Since the discovery of iron-based superconductors[1–4], there has been considerable controversy over the choice of the appropriate microscopic Hamiltonian[5, 6]. The major reason behind such a controversy is on the complicated multi-d-orbital electronic structure of Fe-As or Fe-Se layers. Although the electronic structure has been studied in models constructed by using different number of orbitals, ranging from minimum two orbitals[7] to all five d orbitals[8, 9], a general perception has been that any microscopic model composed of less than all five d-orbitals and ten bands is insufficient[6].

Such a perception has blocked the path to understand underlining superconducting mechanism because of the difficulty in identifying main characters which are responsible for high  $T_c$ . In particular, we have two families of high temperature superconductors, iron-pnictides[1–3] and electron-overdoped iron-chalcogenides[4], with distinct Fermi surface topologies[10–13]. Conventional analyses and models which deeply depend on Fermi surfaces fail to provide a satisfying answer. Moreover, it has been also difficult to understand robust properties revealed in various spectroscopic methods. One of the properties observed by angle-resolved photoemission microscopy (ARPES) in iron-pnictides is that the superconducting gap on different Fermi surfaces is nearly proportional to a simple form factor  $|\cos k_x \cos k_y|$  defined in reciprocal space. This form factor has been observed in both 122[13–16] and 111[17, 18] families of iron-pnictides. In models with above complicated band structures and multi-orbitals, many theoretical calculations based on weak coupling approaches have shown that the gap functions are very sensitive to detailed band structures and vary significantly when the doping changes[6, 19–23]. The robustness of the form factor has been argued to favor strong coupling approaches which emphasize the effective antiferromagnetic (AFM) next nearest neighbour (NNN) exchange coupling  $J_2$  in Fe layers[24–30] as a primary source of pairing force. However, realistically, it is very difficult to imagine such a local exchange interaction remains identical between all d-orbital electrons.

To answer these challenges, we start to ask whether there is an unidentified important electronic structure in a different gauge setting. Giving a translational invariant Hamiltonian that describes the electronic band structure of a Fe square lattice as shown in Fig.1(a),

$$\hat{H}_0 = \sum_{ij,\alpha\beta,\sigma} t_{ij,\alpha,\beta,\sigma} \hat{c}_{i\alpha,\sigma}^+ \hat{c}_{j\beta,\sigma} \quad (1)$$

where  $i, j$  label Fe sites,  $\alpha, \beta$  label orbital and  $\sigma$  labels spin, we perform the following gauge transformation  $\hat{U}$ , which add a minus sign to all Fermionic operators  $\hat{c}_{i\alpha,\sigma}$  at each

site  $i$  marked by red in Fig.1(b). After the transformation, the Hamiltonian becomes  $\hat{H}'_0 = \hat{U}^\dagger \hat{H}_0 \hat{U}$ . There are two intuitive reasons for choosing this transformation. The first reason is that the transformation transfers the Hamiltonian back to reflect the original translational invariance of Fe-As(Se) layer where one unit includes two Fe-sites even if a true unit cell after the transformation includes four iron sites. This can be easily noticed if we divide Fe-sites to two square sublattice A and B as shown in Fig.1(a). After the transformation, the nearest neighbour (NN) hoppings in A sublattice and B sublattice are opposite. The second reason is that as shown in Fig.1(c,d), this transformation maps an extended S-wave  $\cos(k_x)\cos(k_y)$  pairing symmetry in the original Fe lattice to a familiar d-wave  $\cos k'_x - \cos k'_y$  pairing symmetry in both two sublattices, where  $(k_x, k_y)$  and  $(k'_x, k'_y)$  label momentum in Brillouin zones of the origin lattice and sublattice respectively. A similar mapping has been discussed in one-dimensional iron ladder models[28, 31] to address the equivalence of s-wave and d-wave pairing symmetry. It is important to note that the transformation does not change any Hamiltonians that describe electron-electron interactions and the energy eigenvalues of  $\hat{H}_0$ .

There have been various tight binding models to represent the band structure  $\hat{H}_0$ . In Fig.2, we plot the band structure of  $\hat{H}_0$  and the corresponding  $\hat{H}'_0$  for two different models: a maximum five-orbital model for iron-pnictides[9], and a three-orbital model constructed for electron-overdoped iron-chalcogenides[25]. As shown in Fig.2, although there are subtle differences among the band structures of  $H'_0$ , striking universal phenomena appear in both band models. First, all Fermi surfaces locate around  $X'$ , the anti-nodal points in a standard d-wave superconducting state in the Brillouin zone with respect to the sublattice. This is remarkable because a robust d-wave superconducting state can be argued to be favored in such a Fermi surface topology in the presence of repulsive interaction or NN AFM coupling in the sublattice[27, 32]. If we reversely map to the original gauge, the original Hamiltonian must have a robust s-wave pairing symmetry. Second, The bands previously located in different places of Fermi surface are magically reconnected after the gauge mapping. There are just two bands which connect from lower energy bands to higher energy ones and make contribution to Fermi surfaces. These two bands are nearly degenerated and have an hour-glass like dispersion. Finally, the doping level in each band is close to half filling. Therefore, after mapping, it is clear that the low energy physics is controlled by two band models defined with respect to the sublattice periodicity.

With above observations, we believe the essential physics at Fermi Fermi surface should be controlled by two bands. We move to construct an effective band theory to capture the two bands contributing to Fermi surfaces. Since they are close to degenerate and the contribution of  $d_{x'z}$  and  $d_{y'z}$  orbitals on Fermi surfaces is significant, it is natural for us to call the two orthogonal states that form the effective band structure as  $\tilde{d}_{x'z}$  and  $\tilde{d}_{y'z}$  which share the close symmetry with  $d_{x'z}$  and  $d_{y'z}$ . By closely examining the eigenvectors of the two bands in the five-orbital model, we can find that the distribution of  $d_{x'z}$  and  $d_{y'z}$  in one band is dominated by  $d_{x'z}$  orbitals in A sublattice and  $d_{y'z}$  orbitals in B sublattice and the other mainly includes  $d_{y'z}$  in A sublattice and  $d_{x'z}$  in B sublattice. Therefore, our effective  $\tilde{d}_{x'z}$ , and  $\tilde{d}_{y'z}$  should be divided into two groups to form the base set of the band structure: the first group includes  $\tilde{d}_{x'z}$  in A sublattice and  $\tilde{d}_{y'z}$  in B sublattice and the second group includes  $\tilde{d}_{y'z}$  in A sublattice and  $\tilde{d}_{x'z}$  in B sublattice. As shown in Fig.3 where we only draw the  $d_{x'z}$  and  $d_{y'z}$  orbital components for convenient illustration, this classification naturally reflects the existence of separated upper and lower As(Se) layers in a single Fe-As(Se) layer. One of the groups couples strongly to the p-orbitals of the upper As(Se) layer and the other couples strongly to the lower one. Due to this spacial separation of the p-orbitals in upper and lower layers, the coupling between the two bands is weak, which is the essential reason for our observation of two closely degenerated bands with the sublattice periodicity after the gauge mapping.

Having such a picture in mind, we can construct a tight binding model. As illustrated in Fig.3, if only the NN and NNN hoppings are considered, for each band, the tight band models can be approximated by four hopping parameters  $t_{1x}$ ,  $t_{1y}$ ,  $t_2$  and  $t'_2$ .  $t_{1x,1y}$  describes the NN hopping and  $t_2, t'_2$  are the two NNN hoppings in the Fe lattice. Moreover, the local symmetry structure of a Fe atom is defined by the point group symmetry  $S_4$ . If we define  $t_{1s} = (t_{1x} + t_{1y})/2$ ,  $t_{1d} = (t_{1x} - t_{1y})/2$ ,  $t_{2s} = (t_2 + t'_2)/2$  and  $t_{2d} = (t_2 - t'_2)/2$ , the  $S_4$  symmetry requires the signs of  $t_{2d}$  and  $t_{1s}$  to be opposite between the two bands. With these symmetry constrains, the effective two-band model is then described by

$$\begin{aligned} \hat{H}_{0,eff} = \sum_{k\sigma} [4t_{2s}\cos k_x \cos k_y - \mu] (\hat{c}_{k\sigma}^+ \hat{c}_{k\sigma} + \hat{d}_{k\sigma}^+ \hat{d}_{k\sigma}) + 2t_{1s}(\cos k_x + \cos k_y) (\hat{c}_{k\sigma}^+ \hat{c}_{k\sigma} - \hat{d}_{k\sigma}^+ \hat{d}_{k\sigma}) \\ + 2t_{1d}(\cos k_x - \cos k_y) (\hat{c}_{k\sigma}^+ \hat{c}_{k\sigma} + \hat{d}_{k\sigma}^+ \hat{d}_{k\sigma}) + 4t_{2d}\sin k_x \sin k_y (\hat{c}_{k\sigma}^+ \hat{c}_{k+Q\sigma} - \hat{d}_{k\sigma}^+ \hat{d}_{k+Q\sigma}) \end{aligned} \quad (2)$$

where  $Q = (\pi, \pi)$  and  $\hat{c}_{k\sigma}$ ,  $\hat{d}_{k\sigma}$  are Fermionic operators for the two bands. The construction of the two bands is protected by the  $S_4$  point group symmetry of each iron site. We can add

longer range hoppings to the model to account for better quantitative fitting of experimental results. However, we leave this for future report.

The four eigenvalues of the above Hamiltonian are

$$E_{1\pm} = 4t_{2s}\cos k_x\cos k_y - \mu + 4\sqrt{t_{2d}^2\sin^2 k_x\sin^2 k_y + \left(\frac{t_{1s}(\cos k_x + \cos k_y) \pm t_{1d}(\cos k_x - \cos k_y)}{2}\right)^2} \quad (\text{3})$$

$$E_{2\pm} = 4t_{2s}\cos k_x\cos k_y - \mu - 4\sqrt{t_{2d}^2\sin^2 k_x\sin^2 k_y + \left(\frac{t_{1s}(\cos k_x + \cos k_y) \pm t_{1d}(\cos k_x - \cos k_y)}{2}\right)^2} \quad (\text{4})$$

These dispersions can provide correct band structures near Fermi surfaces for both iron-pnictides and iron-chalcogenides as shown in Fig.4. Each band produces electron pockets at  $M$  from  $E_{1\pm}$  and one hole pocket located at  $\Gamma$  from  $E_{2\pm}$ . The parameters  $t_{2s}$  and  $t_{2d}$  describe the s-wave and d-wave type symmetry hoppings in a sublattice. The shallow band position at  $M$  indicates that  $t_{2s}$  is small, the NNN hopping is mostly d-wave. When other parameters are fixed, reducing  $t_{2s}$  can flatten the dispersion along  $\Gamma - M$  direction of  $E_{2\pm}$  and cause the hole pocket completely vanishes. Therefore, the model can describe both iron-pnictides and electron-overdoped iron-chalcogenides by varying  $t_{2s}$ . These general properties in our model suggest the NNN hopping in each band essentially has a d-wave symmetry and this d-wave symmetry is stronger in electron-overdoped iron chalcogenides than in iron-pnictides. We can also perform the gauge mapping to this Hamiltonian as well. As expected, this band structure provides pockets located at  $X'$  as shown in Fig.4.

Now, we consider the coupling between two bands. In general, the coupling,  $\hat{H}_c$  can either keep the  $S_4$  symmetry or lift the symmetry between the two bands. In the five orbital model, the degeneracy at  $\Gamma$  points are kept. If the  $S_4$  symmetry is forced, the two hole pockets must have four more degenerate points around  $\Gamma$  at Fermi surfaces and they are most likely along two  $\Gamma - X$  directions. In the experimental data by ARPES[14], this is indeed the case. The dispersions of the bands for two hole pockets remain degenerate along these two directions. This suggests that the  $S_4$  symmetry breaking is rather weak. We will detail this study in the future. Here, we just give an example of  $S_4$  symmetry breaking term. If we just include the NN hopping between two bands, the following term leads to strong degeneracy breaking of the hole pockets,

$$\hat{H}_c = 2t_c(\cos k_x + \cos k_y)(\hat{c}_{k\sigma}^+ \hat{d}_{k+Q\sigma} + h.c.). \quad (5)$$

$H_c$  changes the sign under  $S_4$  transformation. Therefore, it breaks the  $S_4$  symmetry.

Since the two bands are very weakly coupled and the unit cell of each band includes two irons, the actual unit cell for the whole system includes four irons. One can notice that the gauge mapping closely matches the  $S_4$  symmetry structure and takes four irons per unit cell. These are two essential reasons why the low energy physics becomes transparent after the mapping. All previous two-orbital models are all not built on the  $S_4$  symmetry[7, 35]. In particular, the previous two-orbital model constructed in[7] strictly obeys the  $C_{4v}$  symmetry, which is the symmetry of the Fe square lattice when As(Se) is ignored. This critical symmetry difference is the reason why the previous model fails to capture the low energy physics and also supports our physical picture of the close degeneracy of the two bands are due to the separations of the two *As(Se)* layers which are controlled by the  $S_4$  symmetry.

By projecting all interactions into these two effective bands, a general effective model that describes iron-based superconductors can be written as

$$H_{eff} = H_{0,eff} + H_c + U \sum_{i,\alpha=1,2} \hat{n}_{i,\alpha\uparrow} \hat{n}_{i\alpha\downarrow} + U' \sum_i \hat{n}_{i,1} \hat{n}_{i,2} + J'_H \sum_i \hat{S}_{i1} \cdot \hat{S}_{i2} \quad (6)$$

where  $U$  describes the effective Hubbard repulsion interaction for each band,  $U'$  describes the one between them and  $J'_H$  describes the effective Hund's coupling. Since two bands couple weakly, we expect  $U$  dominates over  $U'$  and  $J'_H$ . In the first order approximation, the model becomes a single band-Hubbard model near half filling. A similar t-J model can also be discussed within the same context as cuprates[33, 34]. It is clear that the model naturally provides an explanation for the stable NNN AFM exchange couplings  $J_2$  observed by neutron scattering[36–38] and its dominating role in both magnetism and superconductivity[27].

From this model, we are in a position to answer one of the most challenging questions: why is a  $A_{1g}$  pairing a robust result regardless of the presence or absence of the hole pockets and a single form factor  $\cos k_x \cos k_y$  is a close fit to gap functions in iron-pnictides? With repulsive interaction, a sign changed order parameter in superconducting state is usually inevitable. This statement, however, is only true when the hopping parameters follow the same lattice symmetry. Gauge transformation can transfer the phases between superconducting order parameters and hopping parameters. In the case of cuprates, the d-wave order parameter can be transferred to a s-wave form by changing hopping parameters to the d-wave symmetry. In the above model, the NNN hopping parameters are highly anisotropic in each sublattice for each band. In fact, the hopping is close to a d-wave symmetry, rather than a s-wave

symmetry. This is the essential reason why the superconducting order can have a s-wave form and be stable in iron-based superconductors. A simple picture of this discussion is illustrated in Fig.5. In this model, it is clear that the vanishing of the hole pockets in electron-overdoped iron-chalcogenides indicates the hopping is more d-wave like, a case supporting stronger s-wave pairing. The presence of the robust form  $\cos k_x \cos k_y$  stems from the fact that the low energy physics is governed by two weakly coupled and almost degenerated single bands. This can also be easily understood after performing the gauge mapping: all Fermi surfaces locate at d-wave anti-nodal points. The gap function should be  $\cos k'_x - \cos k'_y$  because of the stable AFM  $J_2$  coupling just like cuprates[39].

The model completely changes the view of the origin of the generation of sign-changed  $s^\pm$  pairing symmetry in iron-pnictides, which were argued in many theories that the origin is the scattering between electron pockets at  $M$  and hole pockets at  $\Gamma$  due to repulsive interactions[6, 8]. With the new underlining electronic structure in our model, the analysis of the sign-change should be examined after taking the gauge transformation. In this case, the sign change is driven by scatterings that are between all pockets, including both hole and electron pockets, located at two d-wave anti-nodal points. Therefore, the scattering between electron and electron pockets is also important.

In summary, we have shown the underlining electronic structure, which is responsible for superconductivity at low energy in iron-based superconductors, is essentially a two nearly-degenerated weakly-coupled single-band electronic structure. We have successfully constructed an effective model based on the  $S_4$  symmetry group of a  $Fe - As$  layer and have provided a natural explanation why a robust no-sign changed s-wave in iron chalcogenides can be driven by repulsive interaction. We demonstrate the  $s - wave$  in iron-based superconductors is equivalent to  $d - wave$  in cuprates. A similar conclusion has also been reached in the study of 2-layer Hubbard model[40]. These results strongly support identical microscopic superconducting mechanism for cuprates and iron-based superconductors, including both iron-pnictides and iron-chalcogenides. Our model establishes a new foundation for understanding and exploring properties of iron based superconductors.

*Acknowledgement:* JP thanks H. Ding, D.L. Feng, S. A. Kivelson, P. Coleman, X Dai, Y.P. Wang and F. Wang for useful discussion. JP specially thanks H.Ding, F. Wang and W. Li for the discussion of the symmetry properties of the model. The work is supported by the Ministry of Science and Technology of China 973 program(2012CV821400) and NSFC-

- 
- [1] Kamihara, Y., *et al* *J. Am. Chem. Soc.* **130**, 3296-3297 (2008).
  - [2] Chen, X. H., *et al* *Nature* **453**, 761-762 (2008).
  - [3] Chen, G.F., *et al* *Phys. Rev. Lett* **100**, 247002 (2008).
  - [4] Guo, J. *et al.* *Phys. Rev. B* **82**, 180520 (2010).
  - [5] For a review, Johnston, D. C. *Advances in Physics* **59**, 803 (2010).
  - [6] For a review, Hirschfeld P. J., Korshunov, M. M., Mazin, I.I. arXiv:1106.3702 (2011).
  - [7] Raghu, S., *et al* *Phys. Rev. B* **77** 220503 (2008).
  - [8] Mazin, I. I. *et al.* *Phys. Rev. Lett.* **101**, 057003 (2008).
  - [9] Kuroki, K. *et al*, *Phys. Rev. Lett* **101** 087004.
  - [10] Wang, X.-P. *et al.* *Europhys. Lett.* **93**, 57001 (2011).
  - [11] Zhang, Y. *et al.* *Nature Mater.* **10**, 273-277 (2011).
  - [12] Mou, D. *et al.* *Phys. Rev. Lett.* **106**, 107001 (2011).
  - [13] Ding, H. *et al.* *Europhys. Lett.* **83**, 47001 (2008).
  - [14] Richard P., *et al*, *Report on Progress in Physics*, **74**, 124512 (2011).
  - [15] Zhao L. *et al.* *Chin. Phys. Lett.* **25**, 4402 (2008).
  - [16] Nakayama, K. *et al.* *Europhys. Lett.* **85**, 67002 (2009).
  - [17] Umezawa, K, *et al*, *Phys. Rev. Lett.* **108**, 037002 (2012).
  - [18] Liu, Z.-H., *et al*, *Phys. Rev. B.* **84**, 064519 (2011).
  - [19] Wang, F. *et al.* *Phys. Rev. Lett.* **102**, 047005 (2009).
  - [20] Thomale, Ronny, *et al*, *Phys. Rev. B.* **80**, 180505 (2009).
  - [21] Thomale Ronny, *et al*, *Phys. Rev. Lett.* **107**, 117001 (2011).
  - [22] Chubukov, A. V., Efremov, D. V., & Eremin, I. *Phys. Rev. B.* **78**, 134512 (2008).
  - [23] Cvetkovic V. & Tesanovic, Z. *Phys. Rev. B.* **80**, 24512 (2009).
  - [24] Seo, K., Bernevig B. A. & Hu, J. P. *Phys. Rev. Lett.* **101**, 206404 (2008).
  - [25] Fang, C. *et al.* *Phy. Rev. X* **1**, 011009 (2011)
  - [26] Lu, X, *et al*, *Phy. Rev. B* **85**, 054505 (2012)
  - [27] Hu, Jiangping and Ding, Hong arXiv:1107.1334 (2011).
  - [28] Berg E., Kivelson S. A. & Scalapino D.J., *Phys. Rev.B* **81**, 172504 (2010).



- [29] Si, Q. & Abrahams, E. *Phys. Rev. Lett.* **101**, 076401 (2008).
- [30] Hu, J. P. *et al.* Preprint at <http://arxiv.org/abs/1106.5169> (2011).
- [31] Berg E., Kivelson S. A. & Scalapino D.J., *New J. Phys.* **11**, 085007 (2009).
- [32] Scalapino, D. J. *Science* **284**, 1282 (1999).
- [33] Anderson, P. W. *et al.* *J. Phys. Cond. Mat.* **16** R755-R769 (2004).
- [34] Lee, P. A., Nagaosa, N., & Wen, X. G. *Rev. Mod. Phys.* **78**, 17 (2006).
- [35] D. Zhang, *Phys. Rev. Lett* **103**, 186402 (2009)
- [36] Zhao, J. *et al.* *Nature Phys.* **5**, 555-560 (2009).
- [37] Lipscombe, O. J. *et al.* *Phys. Rev. Lett.* **106**, 057004 (2011).
- [38] Wang, M. *et al.* *Nature Comm.* **2**, 580 (2011)
- [39] Kotliar, G. & Liu, J. *Phys. Rev. B* **38** 5142 (1988).
- [40] Mailer T and Scalapino D, arXiv:1107.0401 (2011).

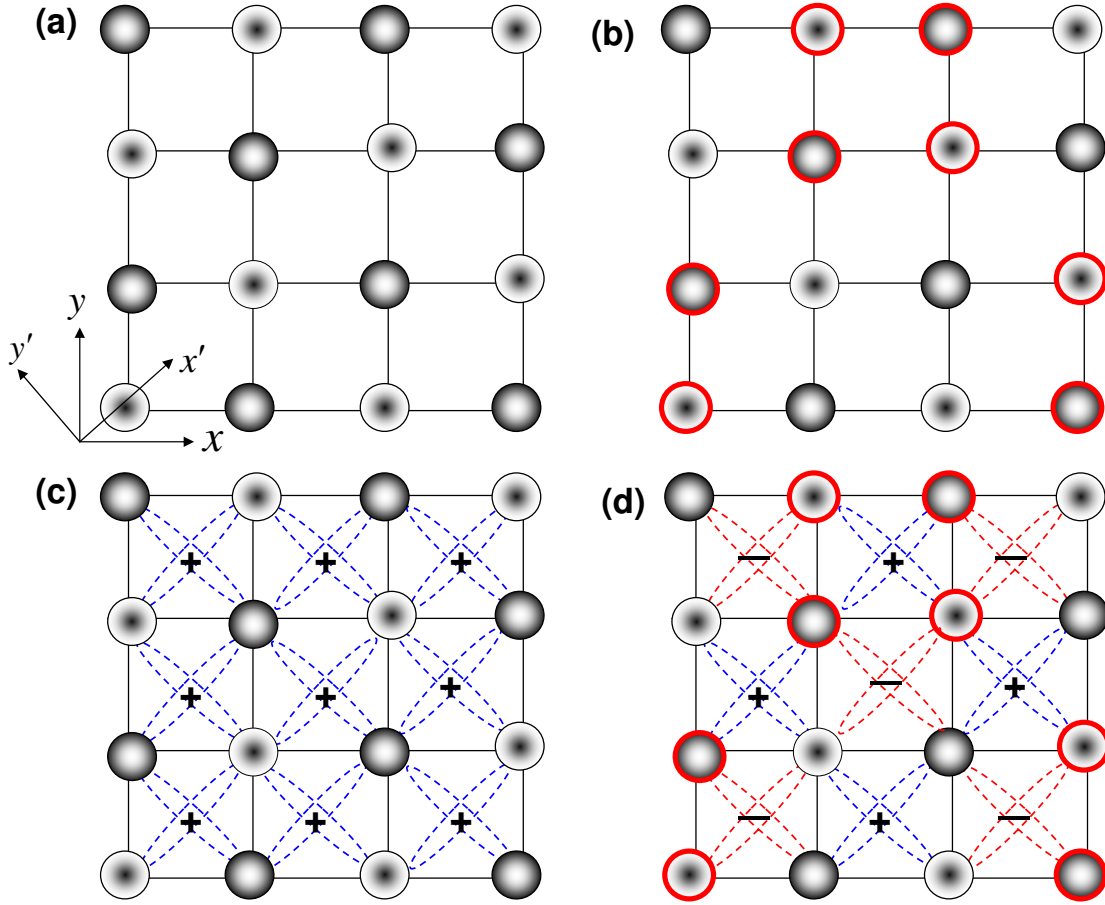


FIG. 1. (a) the square lattice structure of a single iron layer: one cell includes two Fe ions identified with different filled black balls which form two sublattices. We use  $x - y$  coordinate to mark the original tetragonal lattices and  $x' - y'$  to mark the sublattice direction. (b) the gauge transformation is illustrated. The balls with red circles are affected by the gauge transformation. (c) and (d) the mapping from the  $s$ -wave to the  $d$ -wave pairing symmetry by the gauge transformation.

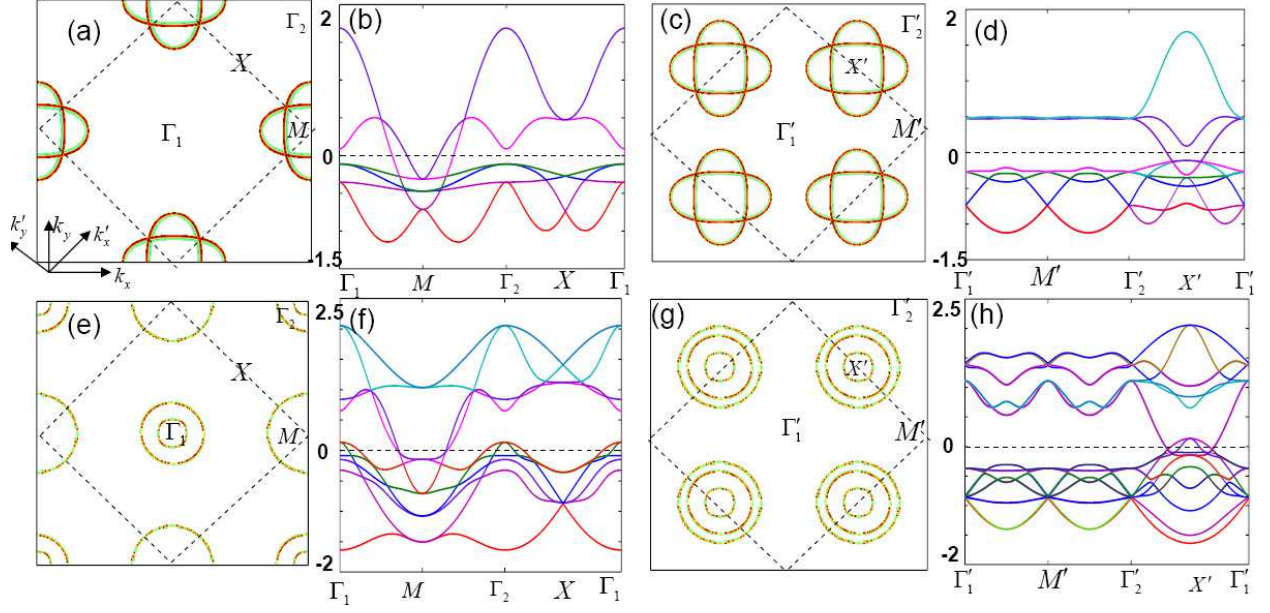


FIG. 2. (Three[25], five[9]) orbital models: (a,e) the Fermi surfaces, (b,f) the band dispersion along the high symmetry lines, (c,g) the Fermi surfaces after the gauge transformation, (d,h) the band dispersion along the high symmetry lines after the gauge transformation. The parameters of the bands can be found in the above two references.

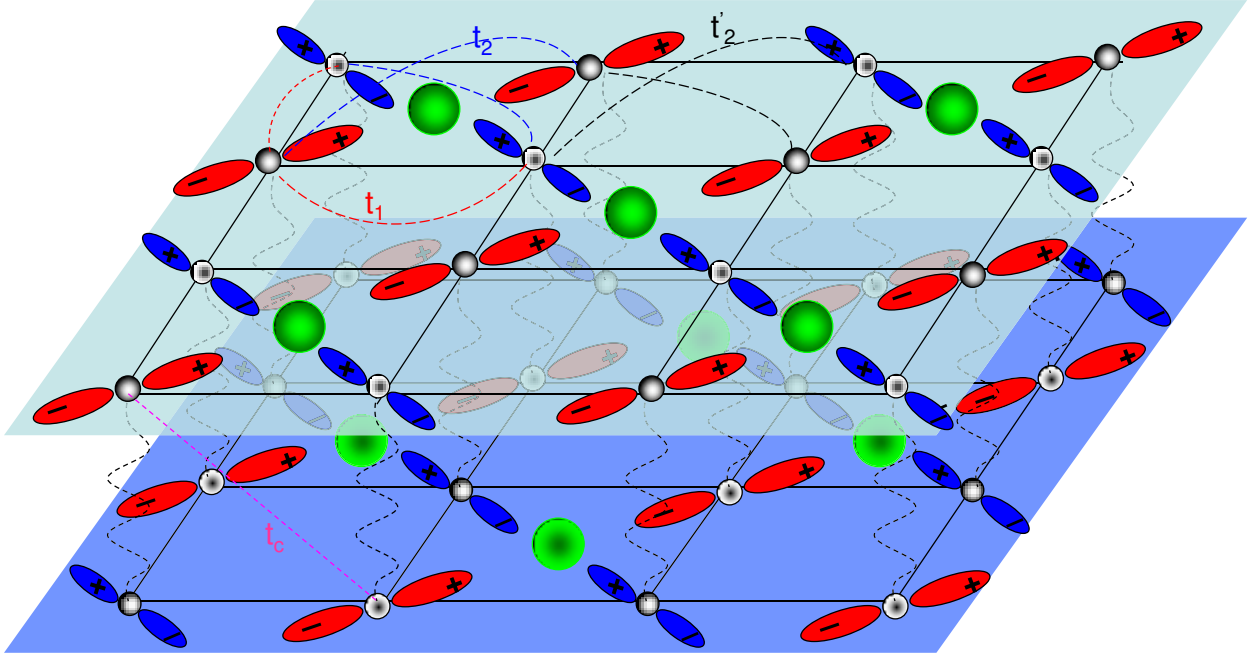


FIG. 3. A sketch of the  $\tilde{d}_{x'z}$  and  $\tilde{d}_{x'z}$  orbitals, their orientations and their coupling into the two As(Se) layers. The hopping parameters are indicated: the nearest neighbor hopping is marked by  $t_1$ , the next nearest neighbor hoppings are  $t_2$  and  $t'_2$  due to the broken symmetry along two different diagonal directions. The coupling between two layers is marked by the nearest neighbor hopping  $t_c$ .

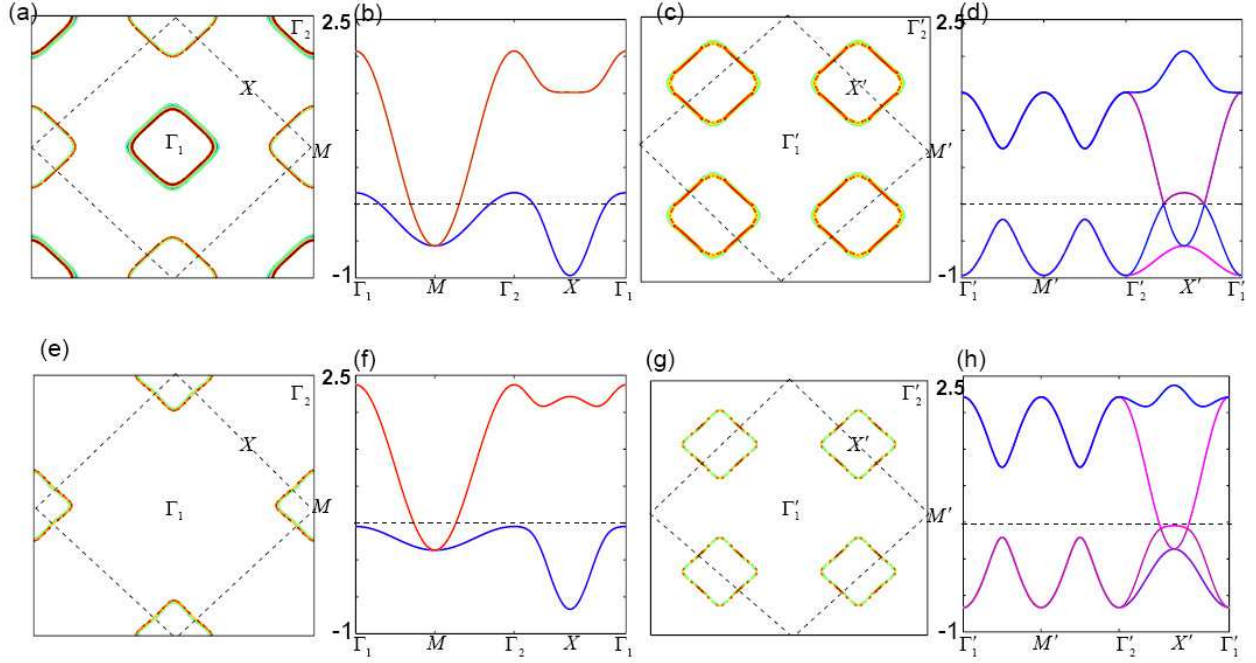


FIG. 4. The Fermi surfaces of each band when  $t_c$  is ignored. The layout exactly follows Fig.2. The parameters are  $t_1 = 0.24$ ,  $t_2 = 0.52$  and  $\mu = -0.273$ . The only different parameter between (a) and (e) is  $t'_2$  with  $t'_2 = -0.1$  in (a) and  $t'_2 = -0.2$  in (e).

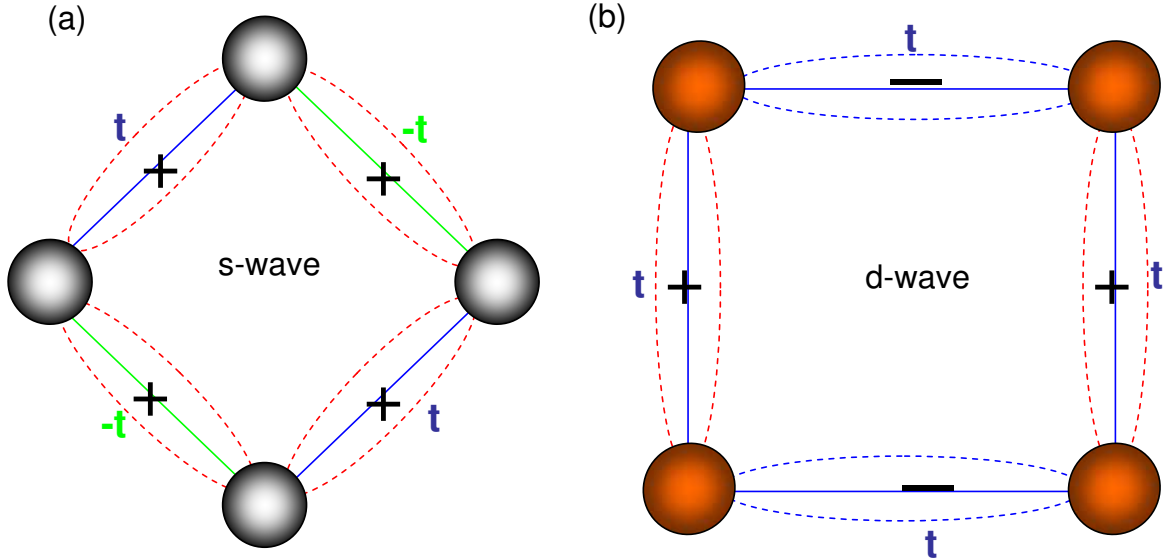


FIG. 5. A sketch of the correlation between the hopping and pairing symmetries for both iron-based superconductors and cuprates.